[CANCER RESEARCH 64, 135–145, January 1, 2004]

α7-Nicotinic Acetylcholine Receptors Affect Growth Regulation of Human Mesothelioma Cells: Role of Mitogen-Activated Protein Kinase Pathway

Sonya Trombino,[1] Alfredo Cesario,[3] Stefano Margaritora,[3] PierLuigi Granone,[3] Giovanni Motta,[4] Carla Falugi,[1] and Patrizia Russo[2]

[1]Department of Biology, University of Genoa, Genoa; [2]Department of Oncogenesis, Unit of Experimental Oncology, National Institute for Research on Cancer Genoa, Genoa; [3]Department of Surgical Science, Division of Thoracic Surgery, Catholic University, Rome; and [4]Department of Integrated Methodologies, Unit of Thoracic Surgery, University of Genoa, Genoa, Italy

ABSTRACT

This study presents data suggesting that both human mesothelioma (cell lines and human mesothelioma biopsies) and human normal mesothelial cells express receptors for acetylcholine and that stimulation of these receptors by nicotine prompted cell growth via activation of nicotinic cholinergic receptors. Thus, these data demonstrate that: (*a*) human mesothelioma cells and human biopsies of mesothelioma as well as of normal pleural mesothelial cells express functionally α-7 nicotinic acethlycholine receptors, evaluated by α-bungarotoxin-FITC binding, receptor binding assay, Western blot, and reverse transcription-PCR; (*b*) choline acetyltransferase immunostaining is present in mesothelioma cells; (*c*) mesothelioma cell growth is modulated by the cholinergic system in which agonists (*i.e.,* nicotine) has a proliferative effect, and antagonists (*i.e.,* curare) has an inhibitory effect, evaluated by cell cloning, DNA synthesis and cell cycle; (*d*) nicotine induces Ca^{+2} influx, evaluated by [$^{45}Ca^{2+}$] uptake, and consequently activation of mitogen-activated protein kinase pathway (extracellular signal-regulated kinase and $p90^{RSK}$ phosphorylation), evaluated by Western blot; and (*e*) apoptosis mechanisms in mesothelioma cells are under the control of the cholinergic system (nicotine antiapoptotic via induction of nuclear factor-κB complexes and phosphorylation of Bad at Ser^{112}; curare proapoptotic via G_0-G_1 arrest $p21^{waf-1}$ dependent but p53 independent). The involvement of the nonneuronal cholinergic system in mesothelioma appears reasonable and open up new therapeutic strategies.

INTRODUCTION

Acetylcholine (ACh), one of the most important examples of a neurotransmitter, represents a phylogenetically old molecule, widely distributed from bacteria to humans. The finding that neuronal nicotinic acetylcholine receptors (nAChRs) are present in nonneuronal cells (Refs. 1–5, recently reviewed in Ref. 5) raised some interesting issues related to their specific activity. In humans, ACh and/or the synthesizing enzyme, choline acetyltransferase (ChAT), have been found in epithelial cells (airways, alimentary tract, urogenital tract, and epidermis), mesothelial (pleura and pericardium), endothelial, muscle and immune cells (mononuclear cells, granulocytes, alveolar macrophages, and mast cells). The widespread expression of nonneuronal ACh is accompanied by the ubiquitous presence of cholinesterase and receptors (nicotinic and muscarinic). In the human placenta, anti-ChAT immunoreactivity is found in multiple subcellular compartments like the cell membrane (microvilli and coated pits), endosomes, cytoskeleton, mitochondria, and in the cell nucleus. These locations correspond with the results of experiments where possible functions of nonneuronal ACh have been identified (proliferation, differentiation, organization of the cytoskeleton and the cell-cell contact, locomotion, migration, ciliary activity, and immune functions; Ref. 5). As a consequence, the presence of nAChRs on these cells strongly suggests that is time to revise the role of ACh in humans.

Different studies have showed that many lung cancer cells expressed nAchRs and that low concentrations of nicotine blocked the induction of apoptosis in these cells. In small cell lung cancer (SCLC) stimulation of the nAChRs by nicotine induced a mitogenic effect antagonized by mecamylamine and α-bungarotoxin (α-BTX; Refs. 6, 7). Furthermore, engagement of nicotine receptors suppresses cell growth inhibition and apoptosis induced by opioids both in SCLC and non-SCLC (NSCLC) cell lines (8–10).

In cholinergic neurons, the neurotransmitter ACh is synthesized from choline and acetyl-CoA by ChAT (1–5), and it is then translocated into synaptic vesicles by the vescicular ACh transporter (1–5). In neurons, choline for the synthesis of Ach is transported by a specific high-affinity choline transporter: CHT1 (1–5). A recent study (10) presents data that SCLC expresses a cholinergic autocrine loop that can regulate cell growth. Such a study demonstrates that: (*a*) genes for all components of an ACh autocrine loop, including ChAT, vescicular Ach transporter, CHT1, nAChR, and muscarinic AChR (mAChR) are expressed in SCLC cells, as well as in neurons cells; (*b*) ChAT is present in biopsies of SCLC and in SCLC cell lines; (*c*) SCLC cells are able to synthesize, secrete, and degrade ACh; and (*d*) SCLC cell growth is modulated by endogenous ACh synthesis. Such work, probably, is the first study that demonstrates that SCLC cells have a cholinergic phenotype and that ACh exerts an autocrine growth factor in human lung tumors. Thus, the identification of a cholinergic autocrine loop by SCLC now provides a framework and rationale for the many studies, in the literature, that nicotine and related compounds stimulate SCLC growth.

The lung is a complex organ consisting of a series of branching tubules and alveoli that are highly vascularized to provide a large gas exchange surface. The respiratory tract is lined by endoderm-derived epithelial cells that differentiate from the foregut endoderm. Commitment and proliferation of respiratory epithelial cells are dependent upon mesenchymal-epithelial interactions, mediated by a number of distinct and intersecting autocrine-paracrine pathways, which, in turn, regulate gene transcription to influence cell fate, proliferation, and function (11). Mesothelium develops from the mesodermal tissue around day 14 of gestation, in humans, with cells that gradually differentiate from round to cuboidal cells to elongated flattened cells that line coelomic cavities (12). Mesothelium is not just a limiting protective layer (pleural mesothelium for lung), but a dynamic cellular structure regulating serosal responses to injury, infection, and disease. Mesothelial cells are biologically active because they can sense and respond to signals within their microenvironment. Mesothelial cells have the property to change between epithelial and fibroblastic phenotypes and more interesting are able to regenerate in a fashion unlike to other epithelial-like surfaces (12). Identifying the genes regulating

Received 6/9/03; revised 9/15/03; accepted 9/29/03.

Grant support: TENDER N° Grant 2000/S 118-076796 "Induction of conformational changes in p53 mutants and modulation of sensitivity to selective anticancer drugs," awarded by European Community, Ispra (VA), Italy (2002) (to P. R.), SENS-PES-TIQLK4-CT-2002-022264 Grant awarded by European Community (Bruxelles, Belgium) (to C. F.), and by a grant from the University of Genoa (Italy), Faculty of Medicine and Surgery (2003) (to G. M.).

The costs of publication of this article were defrayed in part by the payment of page charges. This article must therefore be hereby marked *advertisement* in accordance with 18 U.S.C. Section 1734 solely to indicate this fact.

Requests for reprints: Dr. Patrizia Russo, Department of Oncogenesis, Unit of Experimental Oncology, National Institute for Research on Cancer, Largo Rosanna Benzi 10, I-16132 Genova, Italy. Phone: 39-010-5600212; Fax: 39-010-5600217; E-mail: patrizia.russo@istge.it.

these mechanisms may provide some insight into the development of malignant mesothelioma.

In this study, we have considered the possibility that the growth of mesothelioma cells may be influenced by activation or inactivation of nAChRs. The well-characterized human mesothelioma cell line MSTO-211H was chosen as a model. Our experiments show that MSTO-211H cells as well as other mesothelioma cell lines (MPP-89 and IST-MES-1) and human normal pleural mesothelial cells present α7-nAChRs [evaluated by α-BGT-FITC binding, receptor binding assay, Western blot, and reverse transcription-PCR (RT-PCR)] and has ChAT activity. The addition of nicotine to the culture medium has a growth stimulatory effect [cell cloning, induction of DNA synthesis, and mitogen-activated protein kinase (MAPK) phosphorylation] via induction of antiapoptotic factor [*i.e.*, activation of nuclear factor (NF)-κB complexes, induction of phosphorylation of Bad at Ser^{112}], whereas D-tubocurarine, a classical antagonist of nicotine (13), has a growth inhibitory effect. In three different human biopsies obtained from three different patients suffering from mesothelioma, as well as in two normal mesothelial biopsies obtained from two patients who underwent thoracotomy for nonneoplastic reasons, expression of α7-nAChRs (α-BGT-FITC binding, receptor binding assay, Western blot, and RT-PCR) was demonstrated. Finally, mesothelioma cells in primary culture, obtained by the same biopsies, were potently stimulated to growth by addition of nicotine to the culture.

These data suggest a specific role of the cholinergic system in the growth of mesothelioma.

MATERIALS AND METHODS

Cell and Primary Tumor Human Mesothelioma Cell Cultures

Human mesothelioma cancer cell line MSTO-211H and epidermoid carcinoma skin A431 cell line were obtained by American Type Culture Collection (Manassas, VA). Human mesothelioma cancer cell lines IST-MES-1 and MPP-89 and human ovarian cancer cell line A2774 were a kind gift of Dr. Silvano Ferrini (National Institute for Research on Cancer, Genova, Italy). They were grown in RPMI 1640 (Life Technologies, Inc., Grand Island, NY) supplemented with 10% nonheat-inactivated fetal bovine serum (FBS; Life Technologies, Inc.). Cell counts were determined using a Coulter counter with Channelyzer attachment to monitor cell size (Coulter Electronics, Hialeah, FL). Cell membrane integrity was determined by trypan blue dye exclusion assay.

Tumor tissue samples from patients suffering from mesothelioma were taken from the operating room at room temperature immediately after resection. Normal pleural tissues were taken from patient who underwent surgery for nonneoplastic reasons. The experiments were performed after approval by the Committee of Human Research at the University of Genoa and in accordance with an assurance filed with and approved by the Department of Health (Rome, Italy). The specimens were dissected with scalpels into <5-mm cubes. The pieces of tumor were placed in triple enzyme medium (1× collagenase, 1× hyaluronidase, and 1× DNase; Sigma, St. Louis, MO) in HBSS (Life Technologies, Inc.) with a magnetic bar and were then spun on a stir plate at room temperature for 2–3 h until most of the solid tumor was dissociated. The cells were filtered through a 70-μm nylon cell strainer (Becton Dickinson, Lincoln Park, NJ) and suspended in RPMI 1640 with 10% FBS (Life Technologies, Inc.).

Short-term mesothelial cell cultures were established from stripped pleura obtained from two patients who underwent thoracotomy for nonneoplastic reasons after triple enzyme medium (1× collagenase, 1× hyaluronidase, and 1× DNase; Sigma) disaggregation. Mesothelial cells were grown as primary cultures on fibronectin-coated culture flasks in RPMI 1640 supplemented with 20% heat-inactivated FBS (Life Technologies, Inc.), epidermal growth factor (20 ng/ml), hydrocortisone (1 μM) and insulin (10 μg/ml), transferrin (5 μg/ml), and (50 μg/ml) gentamicin (Life Technologies, Inc.) at 37°C in a humidified 5% CO_2 atmosphere. Fresh complete medium was replaced every 2–3 days until cells were confluent. Upon confluence the cells were lifted by 1× trypsin-EDTA (Life Technologies, Inc.) and subcultured at a 1:2 dilution. The cells were identified as mesothelial cells by immunocytochemical staining with antikeratin antibodies (Dako, Glostrup, Denmark). The third and the fourth passage confluent cultures were used for binding assay and cell growth.

ChAT Immunostaining

Immunoreactivity against ChAT was obtained as follow: fixed cells were rinsed in cold PBS containing 0.5 M glycine, blocked with PBS containing 1% BSA (BSA) and 5% FBS. The incubation was carried out overnight at 4°C in the primary antibody diluted 1:200 in PBS-0.1% BSA −1% FBS. The primary antibody was a polyclonal antibody (AB 143) against ChAT (Biosys), raised in rabbit, and diluted 1:500. After incubation, samples were rinsed with PBS and stained with the secondary antirabbit IgG conjugated to gold particles, diluted 1:100 in PBS containing 0.1% BSA and 1% FBS.

Specificity controls were performed by use of normal serum as primary antibody or by omitting the incubation in the primary antibody. Peroxidase controls were performed by preincubating cells in PBS containing 0.1% H_2O_2 before the incubation in the secondary antibody.

Detection of Nicotine Receptors

nAchR-link molecules were identified by histochemical methods, receptor binding assay, Western blotting, and RT-PCR. Cells were incubated in the dark at 6°C in 10^{-7} M FITC-conjugated α-BTX (Sigma). The snake venom irreversibly binds to the α~ subunit of nAchR and a Leitz microscope, equipped with UV apparatus and filter set for fluorescence, and analyzed the FITC fluorescence.

Binding assays were carried out essentially as described previously (14). Briefly, cells (0.2×10^6 cells/well) were incubated in 0.5 ml of complete medium containing 1 nM [3-[^{125}I]*iodotyrosyl*^{54})] α-BTX (monoiodinated) [buffered aqueous solution; 18.5 MBq/ml, 500 μCi/ml (Amersham Biosciences, Little Chalfont, Buckinghamshire, UK)] with or without a 1000-fold excess of unlabeled α-BTX (Sigma) at 37°C for 2 h. To determine the number ligands/cell, the amount of radioactivity displaced by cold α-BTX was calculated, and the number of ligands for each bound α-BTX was determined.

Tissue specimens were snap frozen in liquid nitrogen and stored at −80°C before RNA extraction. All of the RT-PCR reactions were performed using total RNA: for each sample, $\sim 2 \times 10^6$ cells were homogenized according to a standard protocol (OMNIzol; EuroClone). RNA was precipitated with isopropanol and resuspended in sterile H_2O. Each extract was controlled on agarose gel (1.5% in Tris-Acetic Acid-EDTA buffer) and quantified on a spectrophotometer (Jenway 6405 UV/Vis.). RT-PCR reactions were performed using Moloney murine leukemia virus reverse transcriptase RNase H- (Finnzyme) and DNAzyme II DNA polymerase (Finnzyme): 1 μg of RNA, 2.5 μl of buffer; 0.2 μl of oligodeoxythymidylic acid; and 0.5 μl of deoxynucleoside triphosphates enzyme in 25 μl of total volume. Nicotinic receptor (α7 subunit) mRNA was amplified by using two couples of primers, whereas the other mRNAs were detected directly using cDNA templates. Primers used for amplifications are described in Table 1.

PCR reactions were performed using 1 μg of cDNA, 10 mM Tris-HCl (pH

Table 1 *Primers used for nested PCR*

α7 Nicotinic receptor	Forward primer: 5′-CCT GGC CAG TGT GGA G-3′; reverse primer: 5′-TAC GCA AAG TCT TTG GAC AC-3′	414 bp[b]	T_a = 58°C
α7 Nicotinic receptor[a]	Forward primer: 5′-GAT GAG CAC CTC CTG CAC GG-3′; reverse primer: 5′-GAT GCC GATGGT GCA GAT G-3′	210 bp	T_a = 67°C
Actin	Forward primer: 5′-GTG GGG CGC CCC AGG CAC CA-3′; reverse primer: 5′-CTC CCT AAT GTC ACG CAC GAT TTC-3′	538 bp	T_a = 60°C

[a] Primers used for nested PCR.
[b] bp, base pairs; T_a, temperature of annealing.

8.8 at 25°C), 50 mM KCl, 0.1% Triton X-100, 2 mM $MgCl_2$, 200 μM each deoxynucleoside triphosphate, 0.5 μM each primer, and 1 unit of Taq polymerase (DyNAzyme II DNA polymerase; Finnzymes). The mix was denatured at 94°C for 1 min, annealed at the temperatures described in the table for 1 min, and extended at 72°C for 1 min and 20 s 35 times in PCR-Sprint (Hybaid). The nested PCR for α7 nicotinic receptor was performed amplifying 1 μl of the first product and using the same conditions, but primers were hybridated with higher stringency (1 mM $MgCl_2$). The mix for nested PCR was denatured at 94°C for 1 min, annealed at 67°C for 30 s, and extended at 72°C for 20 s 35 times. The PCR products were loaded on a 1.5% agarose gel (except for α7 nicotinic receptor product that is loaded on a 2.5% high resolution agarose gel) and stained with ethidium bromide.

Measurement of [$^{45}Ca^{2+}$] Influx

[$^{45}Ca^{2+}$] influx into the neurons was measured according to Katsura *et al.* (15). Briefly, MSTO-211H cells were incubated in Ca^{2+}-free and 20 mM HEPES-containing Krebs-Ringer bicarbonate buffer [137 mM NaCl, 4.8 mM KCl, 1.2 mM KH_2PO_4, 1.2 mM $MgSO_4 \cdot 6\ H_2O$, 25 mM $NaHCO_3$, and 10 mM glucose (pH 7.4)] at 37°C for 10 min, and the incubation buffer was discarded to change to fresh and warm (37°C) Ca^{2+}-free HEPES-containing Krebs-Ringer bicarbonate buffer. The reaction was initiated by the addition of 2.7 mM $CaCl_2 \cdot H_2O$ [1.0 μCi of ($^{45}Ca^{2+}$)Cl_2/dish; Amersham Biosciences). After the incubation of the MSTO-11H cells at 37°C for 2min, the radiolabeled Ca^{2+}-containing incubation buffer was discarded followed by five washes with ice-cold HEPES-containing Krebs-Ringer bicarbonate buffer containing 2.7 mM $CaCl_2 \cdot H_2O$ (total volume, 7.5 ml), and the cells were scraped off from a culture dish with 0.5 M NaOH. An aliquot of the alkaline-digested cells was neutralized with equimolar acetic acid and then used to measure radioactivity accumulated in the MSTO-211H cells by liquid scintillation spectrometry. KCl (30 mM) and nicotine were simultaneously added into the incubation buffer with [$^{45}Ca^{2+}$]Cl_2. To examine the effects of the inhibitor D-tubocurarine on the 30 mM KCl- and nicotine-induced alterations in [$^{45}Ca^{2+}$]influx, this agent was added into the incubation buffer 15 s before the addition of 30 mM KCl and nicotine.

Cell Proliferation Assay

All of the experiments for each drug were performed at least twice with a minimum of six replicates/data point/experiment. Mesothelioma cell lines were plated with an eight-channel pipette at 250 cells/well in 96-well plates, whereas human normal mesothelial cells at 500 cells/well in 96-well plates. Drugs were added immediately after cell plating. The final medium volume of each well was 200 μl. Every 3 days; one-half of the volume of the media and drugs were changed after centrifugation of the plates at 1000 rpm for 1 min. At 0, 3, 6, and 9 days of incubation, a 3-(4,5-dimethylthiazol-2-yl)-5-(3-carboxymethoxyphenyl)-2-(4-sulfonyl)-2*H*-tetrazolium-based assay, as previously described (16), was used to measure cell growth. Twenty μl of 3-(4,5-dimethylthiazol-2-yl)-5-(3-carboxymethoxy-phenyl)-2-(4-sulfonyl)-2*H*-tetrazolium reagent (cell Titer 96 Aqueous; Promega Corporation, Madison, WI) were added/well, and absorbance at 490 nm was recorded 2 h later.

Cell Proliferation in Soft Agar Assay

MSTO-211 cells (10^5) or primary human mesothelioma cells (10^6) were cultured in 60-mm dishes in 0.5% low gelling agarose (Sea Plaque) on a base layer of 1% noble agar (Difco) in the presence of indicated amounts of nicotine or D-tubocurarine (added on day 1) or vehicle control in complete medium (according to American Type Culture Collection recommendations), and colonies were scored after 10 days. During the experiment, 0.5 ml of fresh complete medium (with or without drug) were added every 5 days. The cell clonogenic fraction was calculated using the following equation: clonogenic fraction = (colonies counted/number of cells seeded) $\times$ 100.

Rate of DNA Synthesis

The effect of different drugs on the rate of DNA synthesis in human MSTO-211H cells was evaluated using the [^{3}H]thymidine uptake assay. Cells were exposed to increasing concentrations (from 10^{-8} to 10^{-6} M) of nicotine or D-tubocurarine for 3 days and were subsequently pulsed with [^{3}H]thymidine (7 μCi/ml) for 4 h. After DNA precipitation with 10% trichloroacetic acid, the amount of [^{3}H]thymidine incorporated was analyzed by liquid scintillation counting. Values were expressed as the percentage of inhibition of DNA synthesis in the treated, relative to the untreated, cultures.

Flow Cytometry

Cells were plated in log phase in T75 flasks (2700 cells/cm^2) in complete medium for 24 h, then treated for 24 h with nicotine or D-tubocurarine and then counted before flow cytometry. Samples were prepared for flow cytometry essentially as described previously (16). Briefly, cells were washed with 1$\times$ PBS (pH 7.4) and then fixed with ice-cold 70% ethanol. Samples were washed with 1$\times$ PBS and stained with propidium iodide 6 μg/ml (Sigma) containing RNase 2 μg/ml (Sigma) for 30 min at 37°C. Cell cycle analysis was performed using a Becton Dickinson fluorescence-activated cell analyzer and Cell Quest version 1.2 software (Becton Dickinson Immunocytometry Systems, Mansfield, MA). For each sample, at least 20,000 cells were analyzed, and quantitation of the cell cycle distribution was performed using the ModFit LT version 1.01 software (Verity Software House, Inc., Topsham, ME).

Detection of Apoptosis

Apoptosis was detected with different methods: (*a*) cellular DNA fragmentation ELISA assay; and (*b*) internucleosomal DNA fragmentation.

Cellular DNA Fragmentation ELISA Assay. Cellular DNA fragmentation ELISA assay (Boehringer-Mannheim, Mannheim, Germany) was applied to measure apoptotic cell death by detecting of bromodeoxyuridine-labeled DNA fragments in culture supernatant and cytoplasm of cell lysates, according to manufacturer (catalogue no. 1585 045). The assay is based on the quantitative sandwich ELISA principle using two mouse monoclonal antibodies directed against DNA and bromodeoxyuridine, respectively. This allows the specific detection and quantification of bromodeoxyuridine-labeled DNA-fragments. The assay was validated as described previously (17).

Internucleosomal DNA Fragmentation. Internucleosomal DNA fragmentation was shown by the harvesting of total cellular DNA, as described previously (18). Briefly, adherent and detached cells were harvested separately, washed, and lysed with 50 mM Tris (pH 7.5), 10 mM EDTA, 0.5% Triton X-100, and 0.5 mg/ml proteinase K for 2 h at 50°C. Samples were then extracted twice with phenol/chloroform/isoamyl alcohol and precipitated with ethanol. The pellet was resuspended in Tris-EDTA and 10 μg/ml RNase A, and the DNA was separated on a 2% agarose gel.

Western Blot Analysis

Equal amounts of protein were subjected to SDS-PAGE [7.5% SDS-PAGE for MAPK kinase kinase-1 (MEKK-1) or 12.5% SDS-PAGE (for all other antibodies)] and then transferred electrophoretically to a nitrocellulose membrane. Nonspecific binding sites were blocked with blocking buffer containing Tris-buffered saline and 0.1% Tween 20 with 5% nonfat milk powder for 2 h at room temperature, and the blot was incubated with specific antibody in blocking buffer [phospho-p42/p44 MAPK and p42/p44, anti-phospho-p90^{RSK} (Ser^{381}) and p90^{RSK} (New England Biolabs, Beverly MA), with rabbit polyclonal anti-p21$^{waf\text{-}1/CIP1}$, with antimonoclonal p53 and MEKK-1 [(Santa Cruz Biotechnology) polyclonal phospho-specific Bad Ser^{112} or Ser^{136} antibodies (New England Biolabs) or with an antibody that recognizes Bad regardless of its phosphorylation state (New England Biolabs)] at 4°C overnight. After washing, the blot was incubated with an appropriate secondary antibody (Santa Cruz Biotechnology, Santa Cruz, CA) for 1 h at room temperature. After extensive washing, detection was performed using the enhanced chemiluminescence's system with exposure to Hyper film MP.

Gel Mobility Shift Assay

Nucleic extracts and EMSA experiments were performed according to Vikhanskaya *et al.* (14). Briefly, 5 $\times$ 10^5 cells were collected, washed in PBS, and pelleted. Pellet is resuspended in 400 ml of hypotonic buffer [20 mM HEPES (pH 7.9), 10 mM KCl, 0.1 mM EDTA, 0.1 mM EGTA, 1 mM DTT, and 0.5 mM phenylmethylsulfonyl fluoride]. The cells are allowed to swell on ice for 15 min, after which, 25 μl of 18% solution of NP40 are added, and the tubes are vigorously vortexed for 10 s. The homogenate is centrifuged for 30 s in a microfuge. The nuclear pellet is resuspended in 50 μl of ice-cold buffer [20 mM HEPES (pH 7.9), 0.4 M NaCl, 1 mM EDTA, 1 mM EGTA, 1 mM DTT,

and 1 mM phenylmethylsulfonyl fluoride], and the tubes are vigorously rocked at 4°C for 15 min. Nucleic extracts are centrifuged for 5 min in a microfuge at 4°C and supernatant is frozen as aliquots at −70°C. One to 3 mg of each cell treatment were incubated on ice for 30 min in 15 ml of buffer containing 10 mM Tris (pH 7.5), 50 mM NaCl, 1 mM EDTA, 1 mM DTT, 3 mg of poly(deoxyinosinic-deoxycytidylic acid), 2 ml of pab65 (Santa Cruz Biotechnology), or nonspecific antibodies, 1 ng of ^{32}[P] end-labeled oligonucleotide; part of the enhancer sequence from the HIV LTR region (ENH7 from −115 to −81: GCTTGCTACAAGGGACTTTCCGCTGGGGACTTTCC) was added for another 15 min at room temperature. DNA-protein complexes were separated by electrophoresis through 5% native polyacrilamide gel dried and visualized.

Statistical Analysis

Student's *t* test (not significant $P > 0.05$) was used.

RESULTS

Expression and Determination of α7-Nicotinic Acethlycholine Receptors. Neuronal nAChRs are composed of 12 subunits (α2-α10, β2-β4). The curare-mimetic snake α-neurotoxins such as α-BTX (a long neurotoxin from the venom of *Bungarus multicinctus*) are potent competitive inhibitors of AChR function and are highly toxic because of functional blockade of AChRs at the neuromuscular junction (19, 20). α-BTX is used extensively in experiments on the molecular properties of nAChRs and for detection of nAChRs (20). Although nAChRs containing α3 subunit are not sensitive to α-BTX, those containing α7 subunit are, on the contrary, highly sensitive (21). The complexes of α-BTX with α7-nAChRs are stable, whereas those with α9-nAChRs receptors are not and are reversed after 10 min of washing (21). Because our assay of α-BTX-FITC binding entailed three 10-min washes, the binding detected is probably α7. MSTO-211H cells show high green fluorescence only in the presence of α-BTX-FITC, suggesting a binding of α-BTX to the nAChRs (Fig. 1*B*). When the assay was performed on mitotic cells (cells obtained after mitotic shake-off, checked with 4′,6-diamidino-2-phenylindole counterstaining) the binding was stronger (Fig. 1*B*). Human normal nesothelial cells (Fig. 1*C*) show a minor intense green fluorescence in the presence of α-BTX-FITC (suggesting that the binding of α-BTX to the nAChRs was lesser than in MSTO-211H cells). Epidermoid carcinoma of skin A431 cell line was the positive control (Ref. 22; Fig. 1*C*).

To determine the number of ligand sites of α-BTX both MSTO and normal mesothelial cells were subjected to Schatchard analysis of receptor binding characteristics incubating them with variable amounts of ^{125}[I-labeled]-α-BTX in the absence or presence of a

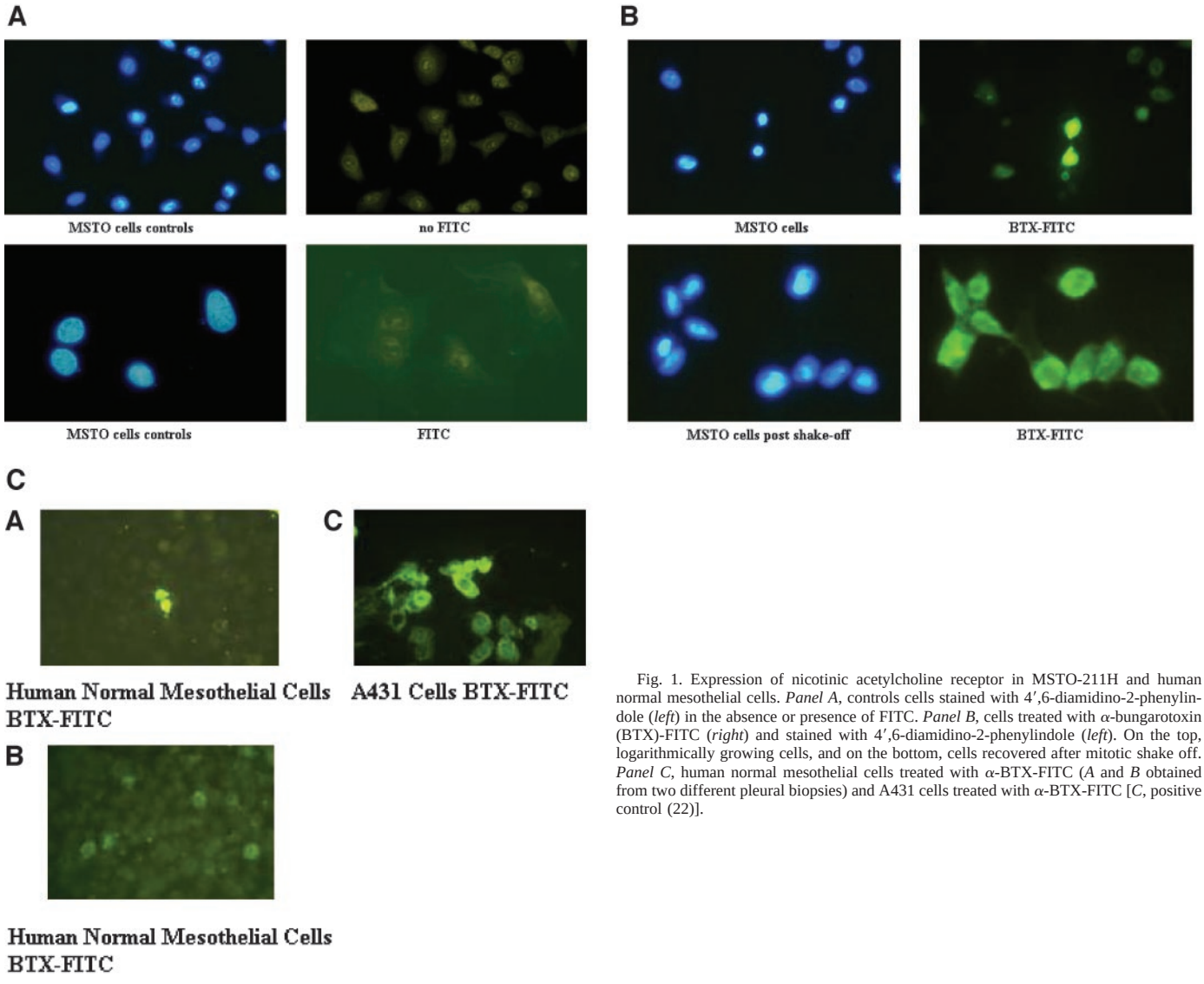

Fig. 1. Expression of nicotinic acetylcholine receptor in MSTO-211H and human normal mesothelial cells. *Panel A*, controls cells stained with 4′,6-diamidino-2-phenylindole (*left*) in the absence or presence of FITC. *Panel B*, cells treated with α-bungarotoxin (BTX)-FITC (*right*) and stained with 4′,6-diamidino-2-phenylindole (*left*). On the top, logarithmically growing cells, and on the bottom, cells recovered after mitotic shake off. *Panel C*, human normal mesothelial cells treated with α-BTX-FITC (*A* and *B* obtained from two different pleural biopsies) and A431 cells treated with α-BTX-FITC [*C*, positive control (22)].

1000-fold excess of unlabeled α-BTX. Table 2 shows that the number of ligand sites were more elevated in MSTO than in human normal mesothelial cells. A431 epidermoid carcinoma cells represents positive control (22).

RT-PCR, Western Blotting, and ChAT Immunoreactivity. Human mesothelioma cells MSTO-211H cell line, as well as two others human mesothelioma cell lines (MPP-89 and IST-MES-1) and two human normal pleural mesothelial cells (obtained from normal tissues), express the α7-nAChR subunit mRNAs (Fig. 2*A*). A431cells represent positive control (22), whereas human ovarian cancer cell line A2774 the negative (Fig. 2*A*) MSTO-211H cells and human mesothelioma samples express proteins for α7-nAChR, as well as samples from normal human pleural mesothelium (Fig. 2*B*). ChAT immunoreactivity in MSTO-211H cells was strong, and mainly localized in the cytoplasm around the nuclei (Fig. 2*C*).

Table 2 *α-BTX-receptor expression on MSTO and human normal mesothelial cells (NMC)*[a]

Cell	n. α-BTX-receptor/cell
MSTO	17,282.5 ± 1,425.3
NMC	5,378.5.5 ± 590
A431	86,899 ± 7,556.5

[a] Results are the mean ± SE from at least duplicate experiments.

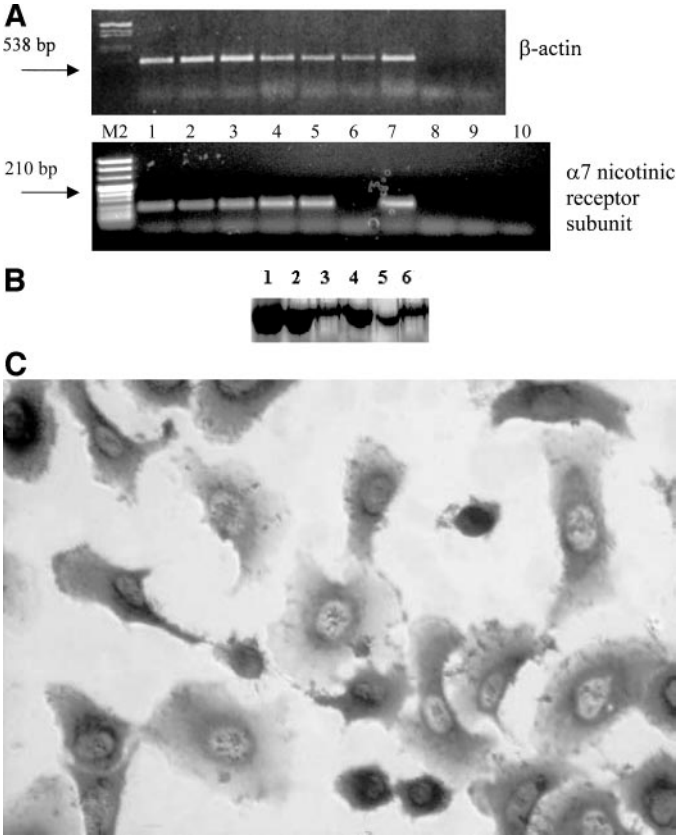

Fig. 2. Expression of α7-nicotinic acetylcholine receptor (nAChR) in mesothelioma cell lines and human normal mesothelial cells. *A*, PCR amplification of α7-nAchR from MSTO-211H mRNA. *M1:* λ DNA *Hin*dIII/*Eco*RI digest; *M2:* marker XIII. *Lane 1*, MSTO-211H mesothelioma cell line; *Lane 2*, IST-MES-1 mesothelioma cell line; *Lane 3*, MPP-89 mesothelioma cell line; *Lane 4*, normal mesothelium, sample no. 1; *Lane 5*, normal mesothelium, sample no. 2; *Lane 6*, A2774 human ovarian cancer cell line (negative control); *Lane 7*, A431 epidermoid carcinoma skin cell line (positive control, Ref. 22); *Lane 8*, control without reverse transcription; *Lane 9*, water (PCR for β-actin); and *Lane 10*, water (PCR for α7-nAchR). *B*, Western blot. Proteins were extracted from human biopsies obtained from two patients who underwent thoracotomy for nonneoplastic reasons (*Lanes 1* and *2*) from three different patients suffering from mesothelioma (*Lanes 3–5*), and from MSTO-211H cells (*Lane 6*). *C*,); choline acetyltransferase immunostaining in MSTO-211H cells.

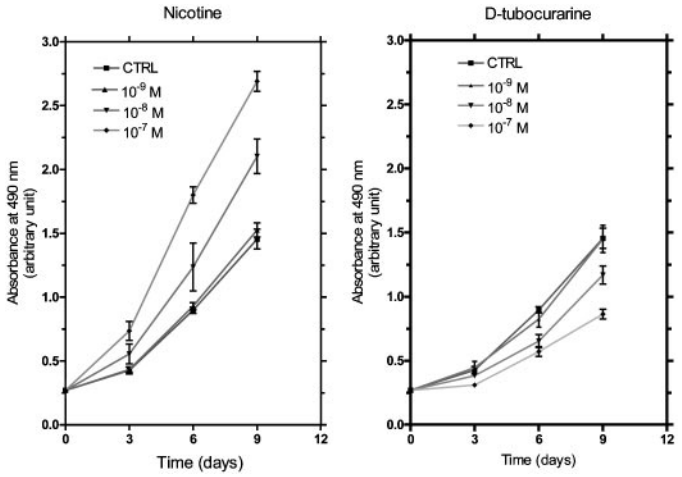

Fig. 3. Effect of modifying cholinergic signaling on MSTO-211H cell growth. MSTO-211H cells were plated in 96-well culture plates (250 cells/well) and cell proliferation measured after specified drug treatments. Cell numbers were measured at 0, 3, 6, and 9 days with the 3-(4,5-dimethylthiazol-2-yl)-5-(3-carboxymethoxy-phenyl)-2-(4-sulfonyl)-2*H*-tetrazolium assay as described in "Materials and Methods." Each point represents the mean ± SE of at least two independent experiments performed in triplicate. $P < 0.05$ by Student's *t* test for 10^{-7} M nicotine or D-tubocurarine (after 3, 6, and 9 days), $P < 0.05$ for 10^{-8} M nicotine or D-tubocurarine (after 6 and 9 days), and $P > 0.05$ for 10^{-9} M nicotine or D-tubocurarine (after 3, 6, and 9 days).

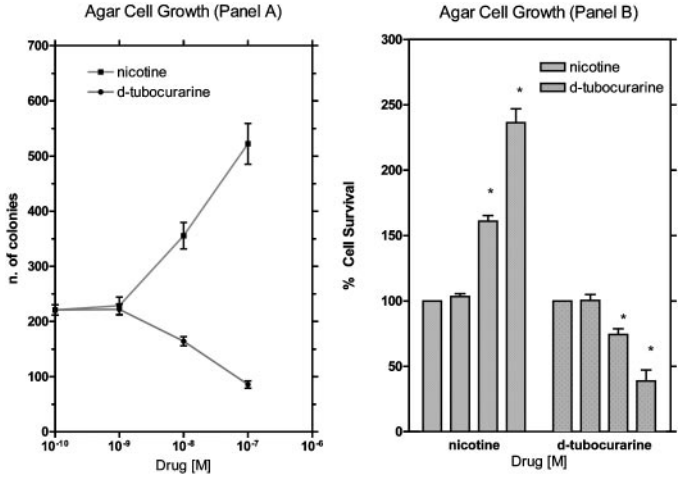

Fig. 4. Effect of modifying cholinergic signaling on MSTO-211H cell growth. MSTO-211H cells were plated in 6-well culture plates on soft agar, and cell proliferation was measured after specified drug treatments. Cell colonies were counted after 10 days. Concentrations were: control, 10^{-8} M; 10^{-7} M, and 10^{-6} M starting from the left. *, $P < 0.05$ by Student's *t* test. Each point represents the mean ± SE of at least four independent experiments performed in triplicate.

Regulation of Mesothelioma Cell Lines Growth. The role of ACh in regulating MSTO-211H cell growth was determined using nAChR agonists (nicotine) or antagonists (D-tubocurarine) in 3-(4,5-dimethylthiazol-2-yl)-5-(3-carboxymethoxy-phenyl)-2-(4-sulfonyl)-2*H*-tetrazolium assay. As shown in Fig. 3, nicotine-stimulated MSTO-211H cells to proliferate in a concentration-dependent and time-dependent manner. A concentration of 10^{-7} M nicotine significantly enhanced MSTO-211H cell growth at 3, 6, and 9 days ($P < 0.05$); a concentration of 10^{-8} M significantly affected cell growth at 6 and 9 days ($P < 0.05$), whereas the concentration of 10^{-9} M was ineffective ($P > 0.05$).

On the contrary, the nAChR antagonist D-tubocurarine inhibited MSTO-211H cell growth in a concentration-dependent and time-dependent manner (Fig. 3). A concentration of 10^{-7} M D-tubocurarine significantly inhibited MSTO-211H cell growth at 3, 6, and 9 days

($P < 0.05$). A concentration of 10^{-8} M D-tubocurarine significantly inhibited MSTO-211H cell growth only at 6 and 9 days ($P < 0.05$). The concentration of 10^{-9} M D-tubocurarine did not inhibit cell growth ($P > 0.05$).

Clonogenic assay performed in soft agar, basically, confirmed the 3-(4,5-dimethylthiazol-2-yl)-5-(3-carboxymethoxy-phenyl)-2-(4-sulfonyl)-2*H*-tetrazolium data (Fig. 4). When two mesothelioma cell lines MPP-89 and IST-MES-1 were exposed to 10^{-7} M nicotine over 9 days, they were stimulated to grow; the effect was statistically significant ($P < 0.05$) after 6 and 9 days (Fig. 5, *left*).

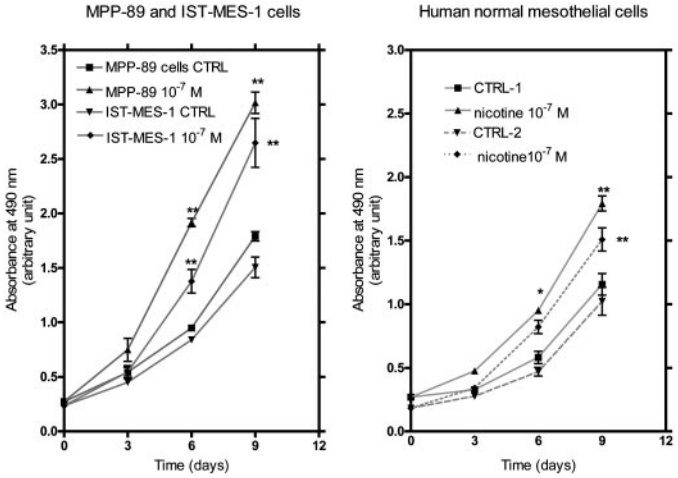

Fig. 5. Effect of modifying cholinergic signaling on mesothelioma (MPP-89 and IST-MES1, on the left) and human normal mesothelial (two cellular samples obtained from two different pleural biopsies, on the right) cell growth. Cells were plated in 96-well culture plates (250 cells/well), and cell proliferation was measured after specified drug treatments. Cell numbers were measured at 0, 3, 6, and 9 days with the 3-(4,5-dimethylthiazol-2-yl)-5-(3-carboxymethoxy-phenyl)-2-(4-sulfonyl)-2*H*-tetrazolium assay as described in "Materials and Methods." Each point represents the mean ± SE of at least two independent experiments performed in triplicate. *, $P < 0.05$; **, $P < 0.01$, compared with the control value by Student's *t* test.

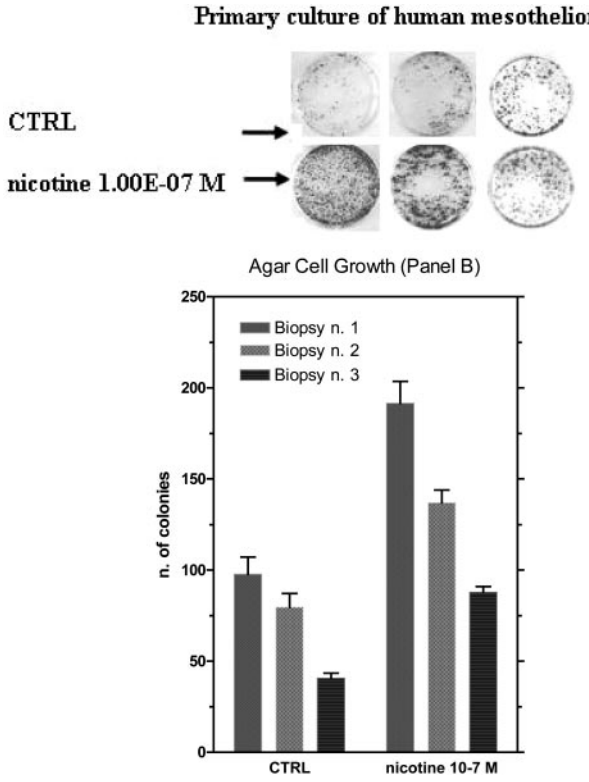

Fig. 6. Effect of modifying cholinergic signaling on human mesothelioma cells obtained by human biopsies. Cells were plated on soft agar in the presence or absence of nicotine 10^{-7} M. Cell colonies were counted after 10 days of continuous exposure. *A*, picture of colonies; *B*, number of colonies, $P < 0.001$ by Student's *t* test. Each *bar* represents the mean ± SE of at least two independent experiments performed in triplicate.

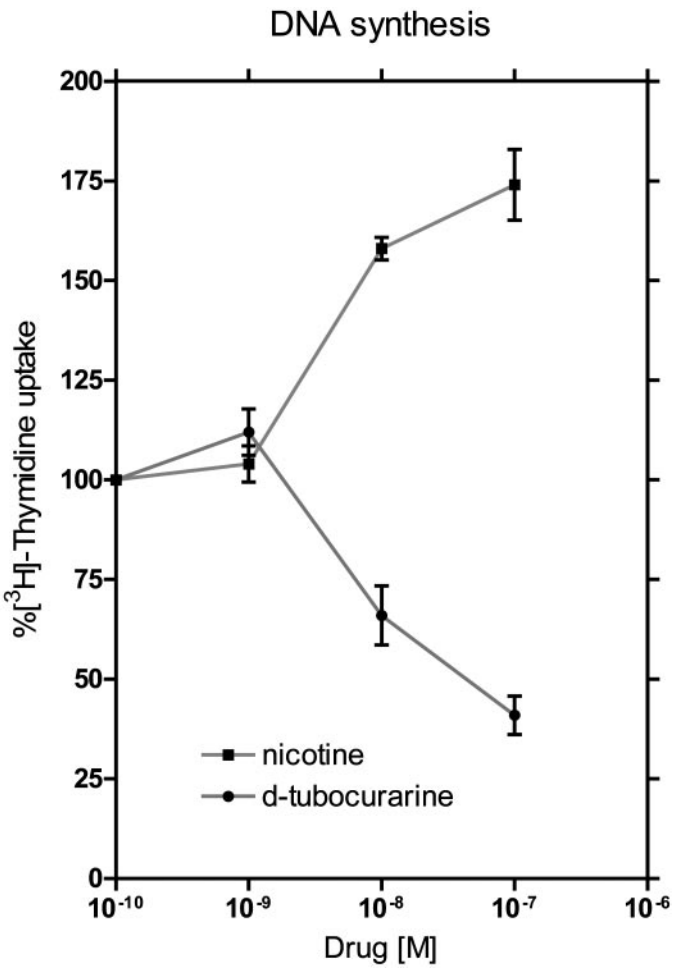

Fig. 7. Kinetics of DNA synthesis in MSTO-211H cells. Cells were treated for 24 h and analyzed by 10-min pulses with 1 μCi/ml [methyl-^{3}H] thymidine (80.9 Ci/mmol) followed by trichloroacetic acid precipitation at different times after drug removal. Mean ± SE of two independent experiments performed in duplicate.

Regulation of Mesothelioma Cell Growth. When mesothelioma cells, obtained by human biopsies, were plated as primary culture in soft agar in the presence of nicotine 10^{-7} M they were stimulated to proliferate ($P < 0.05$; Fig. 6).

Regulation of Human Normal Mesothelial Cell Growth. When human normal mesothelial cells, obtained by thoracotomy, were plated in the presence of nicotine 10^{-7} M, they were stimulated to proliferate, although in an extent lesser than cancer cells (Fig. 5, *right*).

DNA Synthesis. The effect of the two drugs nicotine or D-tubocurarine on the rate of DNA synthesis of the human mesothelioma MSTO-211H cells was also examined using the thymidine uptake assay. As shown in Fig. 7, nicotine treatment resulted in a significant increase in the rate of DNA synthesis in a dose-dependent manner. After 24 h of exposure to the drug (at doses of 10^{-7} and 10^{-9} M), there was a ~70% increase of the rate of DNA synthesis. D-Tubocurarine, treatment (at doses of 10^{-7} and 10^{-9} M for 24 h), on the other hand, resulted in a significant decrease in the rate of DNA synthesis in a dose-dependent manner (Fig. 7), with a ~55% decrease of the rate of DNA synthesis.

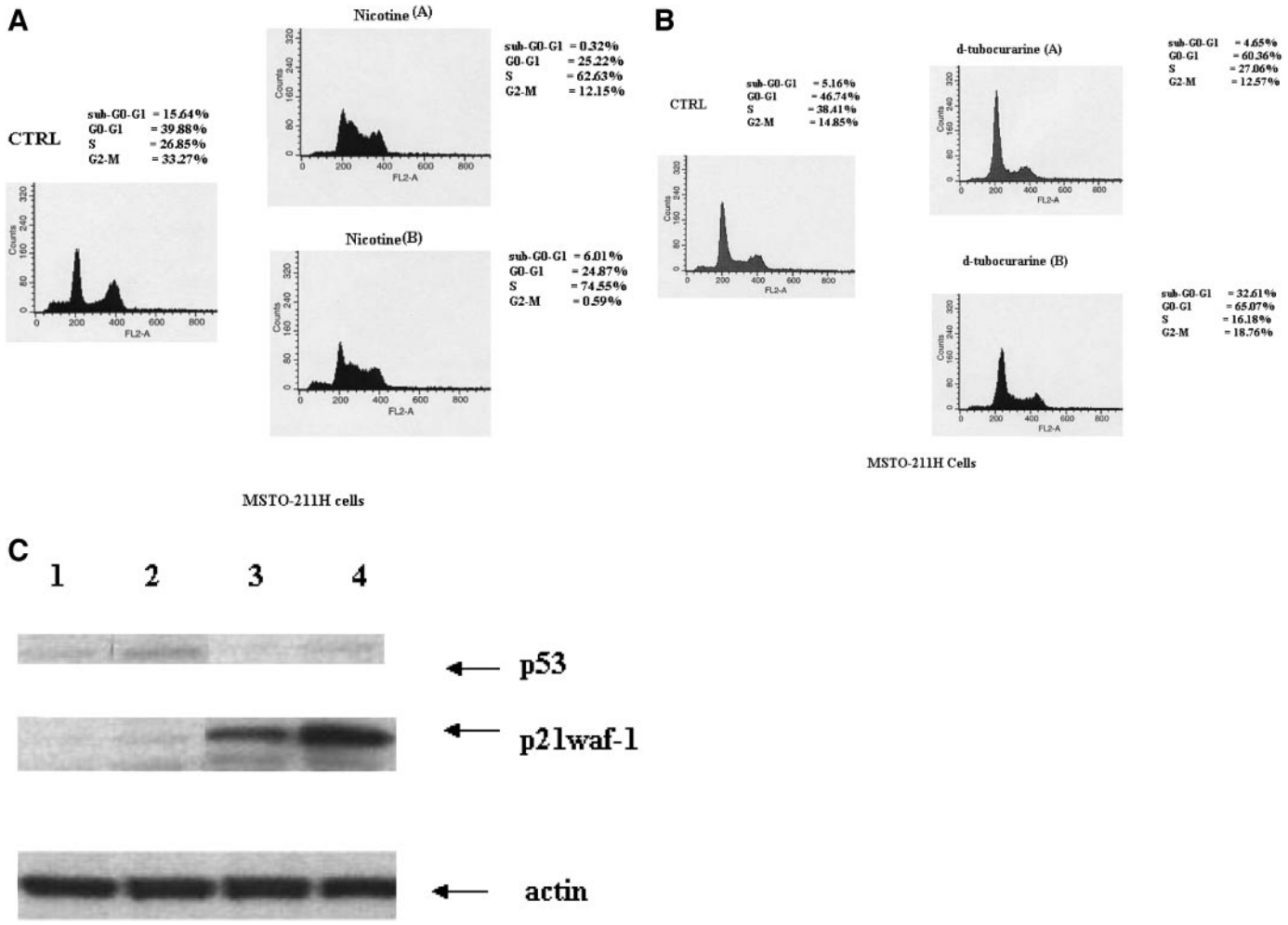

Fig. 8. Cell cycle response to nicotine (*panel A*) or D-tubocurarine (*panel B*) after 24 h of exposure in MSTO-211H human mesothelioma cell line. *Panel A:* flow cytometry profiles of exponential control cells (CTRL); cells treated with nicotine 10^{-8} M (*A*) or 10^{-7} M (*B*). $P < 0.05$ compared with the control value by Student's *t* test. *Panel B:* flow cytometry profiles of: exponential control cells (CTRL); cells treated with D-tubocurarine 10^{-8} M (*A*) or 10^{-7} M (*B*). $P < 0.05$ compared with the control value by Student's *t* test. Data are representative of three replicate experiments yielding similar results. *Panel C:* from the same pool of cells proteins were extracted and separated by SDS-PAGE, transferred to nitrocellulose, and probed with antibodies directed against p53 and p21 $^{waf-1}$. *Lane 1*, control (CTRL); *Lane 2*, nicotine 10^{-7} M; *Lane 3*, D-tubocurarine 10^{-8} M; and *Lane 4*, D-tubocurarine 10^{-7} M. Data are representative of three replicate experiments yielding similar results.

Cell Cycle. To gain insight into the mechanisms of cell growth stimulation or inhibition induced by nicotine or D-tubocurarine, respectively, their possible effect on cell cycle was studied by flow cytometry. The same pool of cells assayed for DNA synthesis was examined by flow cytometry. Fig. 8 shows that nicotine strongly enhanced the percentage of cells accumulated in the S phase of the cell cycle in a dose-dependent fashion [10^{-7} M and 10^{-8} M (Fig. 8, panel A)]. D-Tubocurarine, at the highest concentration (10^{-7} M), induced cells to accumulate in G_0-G_1 and in a sub-G_0-G_1 fraction (statistically significant $P < 0.05$). Thus, D-tubocurarine, but not nicotine, induced $p21^{waf-1}$ (Fig. 8, panel C) expression in a dose-dependent manner. Both two drugs did not induce p53 (Fig. 8, panel C).

Effects on MAPK. Heusch and Maneckjee (23) have provided evidence that nicotine, at a concentration of 10^{-6} M or less, activates the MAPK signaling pathway in lung cancer cells, in particular extracellular signal-regulated kinase (ERK2). According to this observation, effects on ERK activity was investigated after 24 h of treatment with nicotine or D-tubocurarine (at concentration of 10^{-7} M and 10^{-8} M). Nicotine increased strongly the level of phospho-p44/42 MAPK (ERK) (Fig. 9, panel A, *Lanes 2* and *3*). On the contrary, D-tubocurarine reduced the levels of phospho-ERK (Fig. 9, panel A, *Lanes 4* and *5*). Nicotine, but not D-tubocurarine, in a dose-dependent-manner, increases the expression of the upstream to MAPK protein MEKK-1 (Fig. 9, panel B, *Lanes 3–5*). Moreover, nicotine induced, in a concentration-dependent manner, an increase in the expression of the phosphorylated $p90^{RSK}$, a target of ERK1/2, which seems to play a role in cell proliferation (Refs. 24; Fig. 9, panel C, *Lanes 3* and *4*). D-Tubocurarine, at the highest concentration, on the contrary, did not affect the expression of phosphorylated $p90^{RSK}$ (Fig. 9, panel C, *Lane 2*).

Effect of Exposure to Nicotine or D-Tubocurarine on 30 mM KCl-Induced [$^{45}Ca^{2+}$] Influx Into the MSTO-211H Cells. Because nicotine potently stimulates MAPK activity through a Ca^{2+}-activated mechanism (6, 25–28), the effects of the duration of nicotine (10^{-7} M) exposure on 30 mM KCl-evoked [$^{45}Ca^{2+}$] influx has been examined. The increase in 30 mM KCl-induced [$^{45}Ca^{2+}$] influx was found to be dependent on the duration of the exposure to 10^{-7} M nicotine (Fig. 10*A*). The influx attained its plateau 24 h after the exposure, and a similar extent of influx was thereafter maintained up to 72 h (Fig. 10*A*). On the other hand, the basal [$^{45}Ca^{2+}$] influx was not altered during continuous exposure to nicotine (Fig. 10*A*). We examined effects of 24-h exposure to various concentrations of nic-

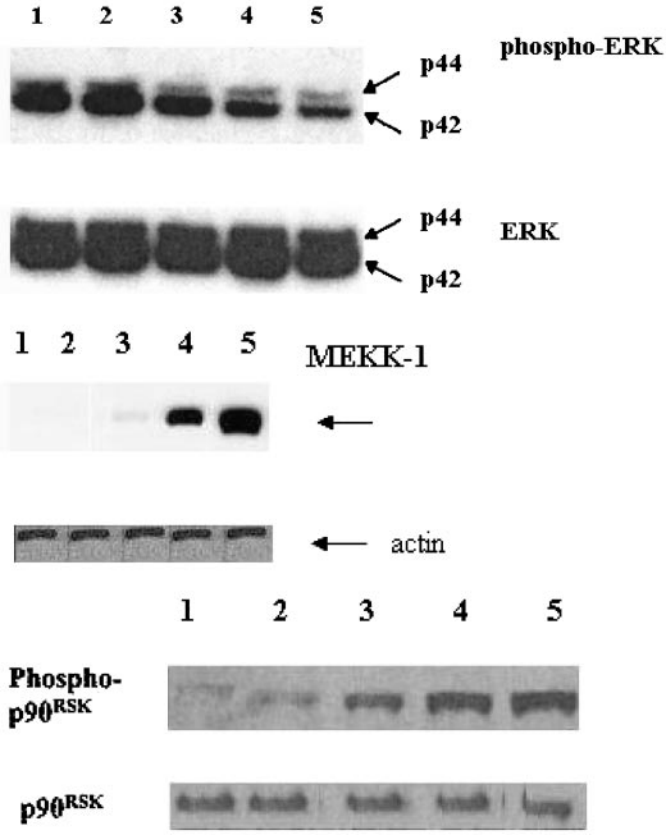

Fig. 9. Logarithmically growing MSTO-211H cells were exposed to different drugs for 24 h, after which, proteins were separated by SDS-PAGE, transferred to nitrocellulose, and probed with antibodies directed against: *A*, phospho-extracellular signal-regulated kinase (ERK)1/2 and total ERK1/2. *Lane 1*, nicotine 10^{-8} M; *Lane 2*, nicotine 10^{-7} M; *Lane 3*, control (CTRL); *Lane 4*, D-tubocurarine 10^{-8} M; and *Lane 5*, D-tubocurarine 10^{-7} M. *B*, mitogen-activated protein kinase kinase-1 (MEKK-1) and β-actin. *Lane 1*, CTRL; *Lane 2*, D-tubocurarine 10^{-8} M; *Lane 3*, D-tubocurarine 10^{-7} M; *Lane 4*, nicotine 10^{-8} M; and *Lane 5*, nicotine 10^{-7} M. *C*, phospho-$p90^{RSK}$ and total $p90^{RSK}$. *Lane 1*, CTRL; *Lane 2*, D-tubocurarine 10^{-7} M; *Lane 3*, nicotine 10^{-8} M; *Lane 4*, nicotine 10^{-7} M; *Lane 5*, 12-*O*-tetradecanoylphorbol-13-acetate (positive control, 100 ng/ml for 4 h). Data are representative of three replicate experiments yielding similar results.

otine on 30 mM KCl-evoked [$^{45}Ca^{2+}$] influx. As shown in Fig. 10*B*, the increase of the 30 mM KCl-induced [$^{45}Ca^{2+}$] influx dependent on nicotine concentration was noticed, and its plateau was observed at nicotine concentrations of 10^{-8} to 10^{-7} M. Whether the significant increase of the 30 mM KCl-induced [$^{45}Ca^{2+}$] influx into the MSTO-211H cells after exposure to 10^{-7} M nicotine for 24 h was attributable to continuous nAChR activation by nicotine was examined by measuring 30 mM KCl-stimulated [$^{45}Ca^{2+}$] influx after concomitant exposure of the cells to nicotine and D-tubocurarine, an antagonist specific for nAChRs. As shown in Fig. 10*C*, this manipulation completely abolished the increase of the KCl-induced [$^{45}Ca^{2+}$] influx. These results indicate that the increased influx by 30 mM KCl after 24-h exposure to 10^{-7} M nicotine is mediated through nAChR activation. These results also imply that ERK phosphorylation by nicotine might be mediated by [Ca^{2+}] influx.

Induction of NF-κB Activity. A key step in the activation of NF-κB is the phosphorylation of its inhibitor by an ubiquitination-inducible multiprotein kinase complex (inhibitor of nuclear factor-κB kinase). MEKK1 induces the site-specific phosphorylation of inhibitor of nuclear factor-κB-α *in vivo* and, most strikingly *in vitro*, can directly activate the inhibitor of nuclear factor-κB-α kinase complex *in vitro* (29). Because nicotine induced MEKK-1, the effect on NF-κB activation has been studied. Nicotine stimulates NF-κB activity in MSTO-211H. (Fig. 11, *Lanes 6* and *7*); D-tubocurarine, on the contrary, did not show any effect (Fig. 11, *Lanes 8–10*, tumor necrosis factor was the positive control).

Induction of Apoptosis. Overexpression of $p90^{RSK}$ in HEK293 cells stimulates Bad phosphorylation at Ser^{112} and Bad-Ser^{112}-phosphorylation effectively blocks Bad-induced cell death (30). Thus, we assessed the ability of nicotine or D-tubocurarine to trigger phosphorylation of Bad at Ser^{112} or at Ser^{136}. A quantitative analysis of the intensity of the bands (Fig. 12) revealed that the apparent $pBAD^{132}$/BAD ratio was, substantially, unaffected by every each drug treatment for 24 h (Fig. 12). On the contrary, nicotine induced phosphorylation of Bad at Ser^{112} (Fig. 12, *Lanes 2* and *5*, apparent $pBAD^{112}$/BAD ratio), whereas D-tubocurarine did not activate phosphorylation of Bad at Ser^{112} (Fig. 12, *Lanes 3*

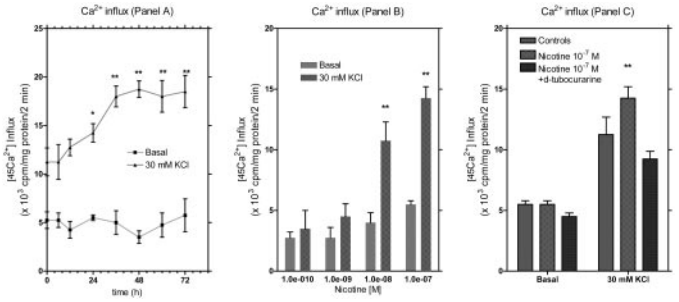

Fig. 10. Effects of 30 mM KCl on [$^{45}Ca^{2+}$] influx into MSTO-211H cells after exposure to nicotine. The MSTO-211H cells were cultured with nicotine at 37°C during 72 h. After incubation of the cells in Ca^{2+}-free incubation buffer for 10 min, the buffer was exchanged to fresh Ca^{2+}-free incubation buffer, and KCl and [$^{45}Ca^{2+}$] Cl2 (1.0 μCi of [$^{45}Ca^{2+}$] Cl2/dish) were simultaneously added into the incubation buffer. The cells were thereafter incubated at 37°C for 2 min, and the reaction was terminated by aspiration of the incubation buffer followed by five washes of the cells with ice-cold incubation buffer containing 2.7 mM $CaCl_2$. The cells were digested with 0.5 M NaOH, and an aliquot of the alkaline-digested cells was subjected to measure radioactivity after neutralization with equimolar acetic acid. Each value represents the mean ± SE obtained from four separate experiments run in triplicate. *A*, time course of changes in 30 mM KCl-stimulated [$^{45}Ca^{2+}$] influx. The cells were cultured with 10^{-7} M nicotine at 37°C for the period indicated. *, $P < 0.05$; **, $P < 0.01$, compared with the control value (without treatment of nicotine; Student's *t* test). *B*, changes in 30 mM KCl-stimulated [$^{45}Ca^{2+}$] influx after exposure to various concentrations of nicotine. The cells were cultured with nicotine at 37°C for 24 h. **, $P < 0.01$, compared with the control value (without treatment of nicotine, Student's *t* test). *C*, effect of D-tubocurarine 10^{-7} M on 30 mM KCl-stimulated [$^{45}Ca^{2+}$] influx. The cells were cultured with nicotine10^{-7} M and D-tubocurarine 10^{-7} M at 37°C for 24 h. **, $P < 0.01$ (Student's *t* test).

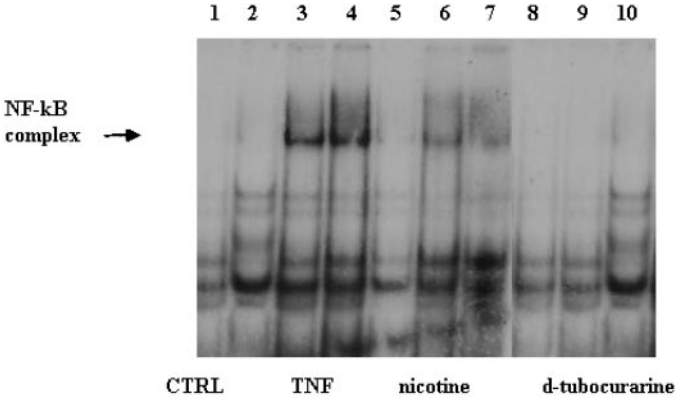

Fig. 11. Gel mobility shift analysis of nuclear factor (NF)-κB complexes. This picture is one representative of three independent experiments. Nucleic extracts of MSTO-211H cells, which were treated with different drugs for 24 h, were incubated with labeled probe containing a NF-κB site. The position of NF-κB complex is shown at the left. *Lanes 1* and *2*, control (CTRL); *Lanes 3* and *4*, recombinant human tumor necrosis factor (TNF) (1000 units/ml; positive control). *Lanes 5–7*, nicotine (10^{-9} M; *Lane 5*), nicotine (10^{-8} M; *Lane 6*), nicotine (10^{-7} M; *Lane 7*). *Lanes 8–10*, D-tubocurarine (10^{-9} M; *Lane 8*), D-tubocurarine 10^{-8} M; *Lane 9*), and D-tubocurarine (10^{-7} M; *Lane 10*).

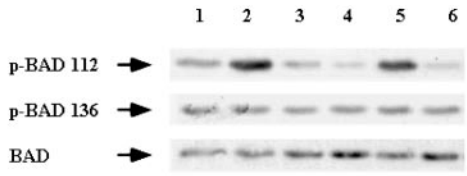

	pBAD^{136}/BAD Arbitrary Unit	pBAD^{112}/BAD Arbitrary Unit
Controls	0.93±0.010	0.83±0.012
Nicotine 10^{-7} M	0.823±0.023	2.103±0.116
Nicotine 10^{-8} M	0.607±0.043	1.273±0.075
Nicotine 10^{-9} M	0.62±0.067	0.55±0.10
D-tubocurarine 10-^{7} M	0.633±0.078	0.55±0.081
D-tubocurarine 10-^{8} M	0.41±0.012	0.243±0.032

Fig. 12. Logarithmically growing MSTO-211H cells were exposed to different drugs for 24 h, after which, proteins were separated by SDS-PAGE, transferred to nitrocellulose, and probed with antibodies directed against polyclonal phospho-specific Bad Ser^{112} and Bad Ser^{136} antibodies or with an antibody that recognizes Bad regardless of its phosphorylation state. Data are representative of three replicate experiments yielding similar results. *Lane 1*, controls; *Lane 2*, nicotine (10^{-7} M); *Lane 3*, D-tubocurarine (10^{-7} M); *Lane 4*, D-tubocurarine (10^{-8} M); *Lane 5*, nicotine 10^{-8} M; and *Lane 6*, nicotine (10^{-9} M). The quantitative analysis of the intensity of the bands was performed, and the table shows in arbitrary units the ratio pBAD^{136}/BAD and pBAD^{112}/BAD.

and *4*, apparent pBAD^{112}/BAD ratio) and, consequently, increased the level of total Bad (Fig. 12, *Lanes 3* and *4*).

As a result of nicotine induced phosphorylation of Bad at Ser^{112} and NF-κB activation, no DNA fragmentation was observed in cells exposed to this drug (Fig. 13). On the contrary, DNA fragmentation started 18 h after addition of 10^{-7} M D-tubocurarine and increased by increasing time of incubation, raising the plateau level after 48 h (Fig. 13). Gel ladder confirmed the induction of DNA-fragmentation related to induction of apoptosis (~180 bp) only in cells treated with D-tubocurarine 10^{-7} M for 48 h (Fig. 14, *Lane 3*, camptothecin was the positive control).

DISCUSSION

This study presents data that human mesothelioma express a cholinergic system, possibly involved in cell growth regulation. Taken together, these data demonstrate that: (*a*) human mesothelioma cell lines (MSTO-211H, MPP-89, and IST-MES1) and human biopsies of mesothelioma, as well as normal mesothelial cells, express α7-nicotinic acethlycholine receptors; (*b*) ChAT immunostaining is present in mesothelioma MSTO-211H cells; (*c*) mesothelioma cell growth, as well as normal mesothelial cells growth, is modulated by the cholinergic system in which agonists (*i.e.*, nicotine) have a proliferative effect, and antagonists (*i.e.*, curare) have an inhibitory effect; and (*d*) apoptosis mechanisms in mesothelioma cells are under the control of the cholinergic system (nicotine antiapoptotic and curare proapoptotic). To our knowledge, this is the first study to demonstrate that mesothelioma cells have a cholinergic phenotype and this phenotype plays a role as growth factor.

The presence of α7-nAChRs was unambiguously demonstrated by the presence of specific mRNA and protein. The functionality of these receptors was proved demonstrating a modulation of growth induced by agonist or antagonist drugs.

Nicotine, by binding to α7-nAChRs, triggers an initial cytosolic influx of sodium (27, 31), creating membrane depolarization that then admits Ca^{2+} to the cytosol through voltage-gated calcium channels. Influx of Ca^{2} inside MSTO-211H cells, after nicotine exposure, was demonstrated, whereas curare, selectively, antagonizes this property.

Ca^{2+} activates two major signaling pathways (protein kinase C and MAPK cascade, respectively), resulting in suppression of physiological process of apoptosis. The precise mechanism by which nicotine increases ERK2 activity is yet to be determined. In PC12 cells, a Ca^{2+} influx induced by carbachol, via nicotinic receptors, activates PYK2 tyrosine kinase, which in turn is responsible for triggering the Ras/MAPK signaling cascade (25, 26). However, the activation of MAPK in the SCLC cell line GLC-8 did not involve PYK2 tyrosine kinase activity (7). Nevertheless, PC12 also showed that Ca^{2+} activates protein kinase C, thereby eliciting the MAPK cascade, initially by serine/threonine phosphorylation and thus activating RAF, which in turn causes phosphorylation and activation of MAP/ERK kinase, MAPK, cAMP-responsive element binding protein kinase, and cAMP-responsive element binding protein (32).

In mesothelioma MSTO-211H cells, after treatment with nicotine and consequent influx of Ca^{2}, the level of MEKK-1 increased, MAPKs are activated, and the level of phosphorylated p90^{RSK} is augmented. As a consequence of MEKK-1 increase, NF-κB complexes are activated. As a result, MSTO-211H cells are pressed on S phase of the cell cycle, the rate of DNA synthesis increased, and cell are pushed to proliferate. Curare shows a completely opposite effect, and exposed cells accumulate in the G_0-G_1 phase of the cell cycle in a p21^{waf-1}-dependent fashion, and eventually, cell growth is inhibited. Both nicotine and curare did not affect p53.

MAPK pathway trough Bad phosphorylation is involved in cell survival at the level of mitochondria (33). Thus, MAPK activates RSK, which in turn catalyzes the phosphorylation of Bad, one Bcl-2 member, at Ser^{112} (33). Induction of Bad phosphorylation on multiple serine residues influences its subcellular distribution from an association with Bcl-$_{xL}$ at the mitochondria to a cytosolic location associated with 14-3-3 molecules. The association of Bad with Bcl-$_{xL}$ is mediated through dimerization of BH3 domains. Phosphorylation of residues in proximity to the BH3 domain of Bad may alter the affinity of Bad for Bcl-$_{xL}$, promoting dissociation. This may relieve Bcl-$_{xL}$ of some influence, allowing protection of cells by apoptosis. Nicotine strongly promotes phosphorylation of Bad at Ser^{112}, whereas curare does not. The phosphorylation at Ser^{136} is predominantly catalyzed by phosphatidylinositol 3-kinase/AKT pathway (33). The observation

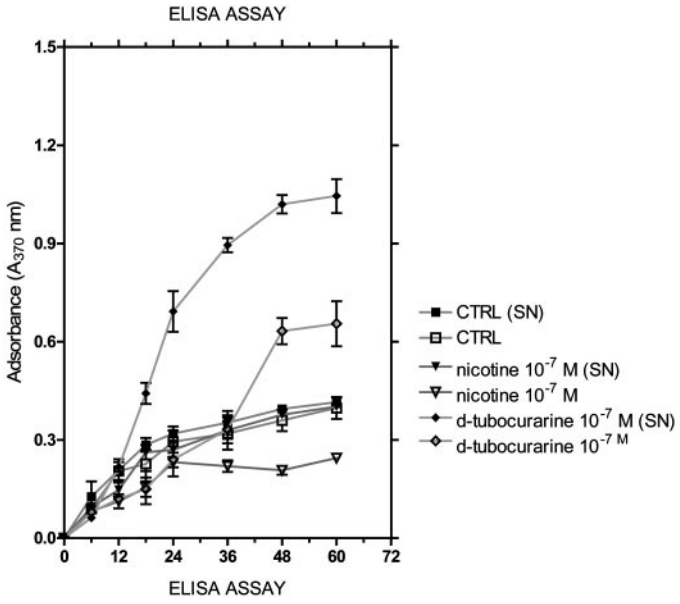

Fig. 13. Kinetics of drug-induced apoptotic cell death in MSTO-211H cells evaluated by ELISA assay. A total of 10^4 cells/well was incubated with nicotine (10^{-7} M) or D-tubocurarine (10^{-7} M) for different times. After the times indicated, 100 μl/well supernatant (SN; *filled symbols SN*) and 100 μl/well lysates (*empty symbols*) were removed and tested by ELISA. Data are expressed as mean ± SE of two independent experiments performed at least in duplicate.

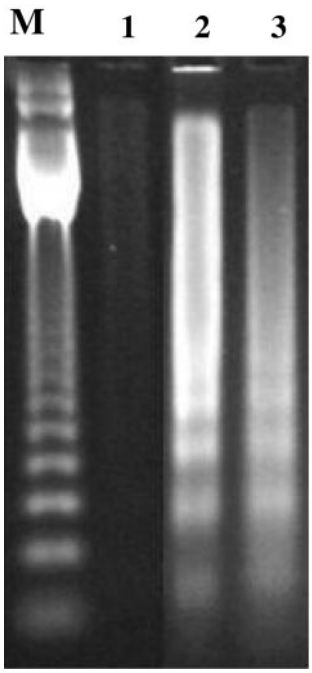

Fig. 14. Induction of apoptosis evaluated by internucleosomal DNA fragmentation (gel ladder). Cells were treated for 48 h with different drugs. Data are representative of three replicate experiments yielding similar results. *Lane 1*, controls; *Lane 2*, nicotine 10^{-7} M; *Lane 3*, D-tubocurarine 10^{-7} M; and *Lane 4*, CPT 10^{-7} M.

that no phosphorylation at Ser^{136} was induced in MSTO-211H cells might imply that the phosphatidylinositol 3-kinase/AKT pathway is not involved.

As a final result Ach agonists such as nicotine pressed cells to proliferate via inhibition of apoptosis, whereas antagonists such as curare blocked cell proliferation both trough a G_0-G_1 arrest mediated by p21 $^{waf-1}$ and consequent induction of apoptosis.

These data support the hypothesis that nonneuronal acethlycholine sensitive receptors play an important role in the regulation of basic cell functions such as gene expression and proliferation. These receptors have been demonstrated, in humans, in normal mesothelial cells (pleura and pericardium; Refs. 1–3, 5 and these data), and it has been proposed that they might represent an universal cell molecule in biological systems, including humans (1–3, 5). The involvement of the nonneuronal cholinergic system in mesothelioma appears reasonable and open up new therapeutic strategies.

Malignant mesothelioma is a highly invasive tumor with a poor prognosis, most patients dying within 18 months of initial diagnosis (34). The mechanisms of mesothelial cell transformation by asbestos have been unclear. Cummins *et al.* (35) showed that the ERKs 1 and 2 of the MAPK cascade is linked causally to the advent of DNA synthesis in alveolar epithelial cells *in vitro* after exposure to asbestos. Work to date (35, 36) suggests that crocidolite asbestos fibers cause activation of ERK1/2 via phosphorylation and aggregation of the epidermal growth factor receptor. After inhalation of chrysotile fibers by mice, increased expression of phosphorylated or activated ERK1/2 is observed by immunoperoxidase staining in cells at the alveolar duct junction where asbestos fibers initially deposit and accumulate. Recently, Ramos-Nino *et al.* (36) have demonstrated that asbestos fibers cause selective and protracted increases in the activator protein-1 family member, Fra-1, a prominent component of the activator protein-1 complex in asbestos-exposed rat leural mesothelial and mesothelioma cells. Moreover, they demonstrated ERK-dependent induction of Fra-1 and a causal relationship between ERK-activation, Fra-1 in activator protein-1 complexes, and mesothelial cell transformation. The reversion to a normal morphology and inhibition of anchorage-independent growth in mesothelioma cells transfected with dnfra-1 conclusively demonstrate that Fra-1 is necessary for the maintenance of mesothelial cell transformation. However, because overexpression of fra-1 in normal rat pleural mesothelial cells did not result in a transformed phenotype, Fra-1 overexpression alone does not appear to be sufficient for conversion to anchorage-independent growth or loss of contact inhibition. More recently, Bocchetta *et al.* (37) showed that SV40 infection of human mesothelial cells directly causes overexpression of Notch-1, a key cell regulatory gene. Notch-1 induction is achieved at the transcriptional level and requires both the SV40 large T-antigen and the small t-antigen. The SV40 tag binds and inhibits protein phosphatase 2A, a protein involved in the dephosphorylation of many protein substrates, including components of the MAPK pathway. Through inhibition of protein phosphatase 2A, a tag may alter the activity of several phosphoproteins, and thus, it may indirectly reinforce mitogenic stimuli acting through MAPK signaling and induce activator protein-1 activity.

By influencing the MAPK pathway, nicotine and D-tubocurarine have a direct effect on a key molecular mechanism that lead to the malignant transformation of mesothelial cells. These findings are relevant to our understanding of the cellular mechanism that influence the growth of mesothelial cells and mesothelioma. Moreover, these data have the potential to lead to preventive/therapeutic approaches aimed at interfering with the activation of the cholinergic receptors on mesothelioma cells.

ACKNOWLEDGMENTS

We thank Dr. Giorgio Tanara (National Institute for Research on Cancer, Genova) for helping us in identifying normal mesothelial and mesothelioma cells obtained by human biopsies with histological and immunocytochemical staining.

REFERENCES

1. Wessler, I., Kirkpatrick, C. J., and Racke, K. Non-neuronal acetylcholine, a locally acting molecule, widely distributed in biological systems: expression and function in humans. Pharmacol. Ther., *77:* 59–79, 1998.
2. Wessler, I., Kirkpatrick, C. J., and Racke, K. The cholinergic 'pitfall': acetylcholine, a universal cell molecule in biological systems, including humans. Clin. Exp. Pharmacol. Physiol., *26:* 198–205, 1999.
3. Wessler, I., Kilbinger, H., Bittinger, F., and Kirkpatrick, C. J. The biological role of non-neuronal acetylcholine in plants and humans. Jpn. J. Pharmacol., *85:* 2–10, 2001.
4. Sharma, G., and Vijayaraghavan, S. Nicotinic receptor signaling in nonexcitable cells. J. Neurobiol., *53:* 524–534, 2002.
5. Wessler, I., Kilbinger, H., Bittinger, F., Unger, R., and Kirkpatrick, C. J. The non-neuronal cholinergic system in humans: Expression, function and pathophysiology. Life Sci., *72:* 2055–2061, 2003.
6. Cattaneo, M. G., D'atri, F., and Vicentini, L. M. Mechanisms of mitogen-activated protein kinase activation by nicotine in small-cell lung carcinoma cells. Biochem. J., *328:* 499–503, 1997.
7. Sher, E., Codignola, A., Passafaro, M., Tarroni, P., Magnelli, V., Carbone, E., and Clementi, F. Nicotinic receptors and calcium channels in small cell lung carcinoma. Functional role, modulation, and autoimmunity. Ann. N. Y. Acad. Sci., *841:* 606–624, 1998.
8. Maneckjee, R., and Minna, J. D. Opioid and nicotine receptors affect growth regulation of human lung cancer cell lines Proc. Natl. Acad. Sci. USA, *87:* 3294–3298, 1990.
9. Maneckjee, R., and Minna, J. D. Opioids induce while nicotine suppresses apoptosis in human lung cancer cells. Cell Growth Differ., *5:* 1033–1040, 1994.
10. Song, P., Sekhon, H. S., Jia, Y., Keller, J. A., Blusztajn, J. K., Mark, G. P., and Spindel, E. R. Acetylcholine is synthesized by and acts as an autocrine growth factor for small cell lung carcinoma. Cancer Res., *63:* 214–221, 2003.
11. Demayo, F., Minoo, P., Plopper, C. G., Schuger, L., Shannon, J., and Torday, J. S. Mesenchymal-epithelial interactions in lung development and repair: are modelling and remodelling the same process? Am. J. Physiol. Lung Cell. Mol. Physiol., *283:* L510–L517, 2002.
12. Mutsaers, S. E. Mesothelial cells: their structure, function and role in serosal repair. Respirology, *7:* 171–191, 2002.
13. Wenningmann, I., and Dilger, J. P. The kinetics of inhibition of nicotinic acetylcholine receptors by (+)-tubocurarine and pancuronium. Mol. Pharmacol., *60:* 790–796, 2002.

14. Vikhanskaya, F., Falugi, C., Valente, P., and Russo, P. Human papillomavirus type 16 E6-enhanced susceptibility to apoptosis induced by TNF in A2780 human ovarian cancer cell line. Int. J. Cancer, *97:* 732–739, 2002.
15. Katsura, M., Mohri, Y., Shuto, K., Hai-Du, Y., Amano, T., Tsujimura, A., Sasa, M., and Ohkuma, S. Up-regulation of L-type voltage-dependent calcium channels after long term exposure to nicotine in cerebral cortical neurons. J. Biol. Chem., *277:* 7979–7988, 2002.
16. Russo, P., Malacarne, D., Falugi, C., Trombino, S., and O'Connor, P. M. RPR-115135, a farnesyltransferase inhibitor, increases 5-FU-cytotoxicity in ten human colon cancer cell lines: role of p53. Int. J. Cancer, *100:* 266–275, 2002.
17. Russo, P., Arzani, D., Trombino, S., and Falugi, C. c-myc down-regulation induces apoptosis in human cancer cell lines exposed to RPR-115135 (C31H29NO4), a non-peptidomimetic farnesyltransferase inhibitor. J. Pharmacol. Exp. Ther., *304:* 37–47, 2003.
18. Solary, E., Bertrand, R., Jenkins, J., and Pommier, Y. Radiolabeling of DNA can induce its fragmentation in HL-60 human promyelocytic leukemic cells. Exp. Cell Res., *203:* 495–498, 1992.
19. Moise, L., Piserchio, A. Basus, J. A., and Hawrot, E. NMR structural analysis of α-bungarotoxin and its complex with the principal α-neurotoxin-binding sequence on the α7 subunit of a neuronal nicotinic acetylcholine receptor. J. Biol. Chem., *277:* 12406–12417, 2002.
20. Antil, S., Servent, D., and Ménez, A. Variability among the Sites by which curaremimetic toxins bind to *Torpedo* acetylcholine receptor, as revealed by identification of the functional residues of α-cobratoxin. J. Biol. Chem., *274:* 34851–34858, 1999.
21. Levandoski, M. M., Lin, Y., Moise, L., McLaughlin, J. T., Cooper, E., and Hawrot, E. Chimeric analysis of a neuronal nicotinic acetylcholine receptor reveals amino acids conferring sensitivity to α-bungarotoxin. J. Biol. Chem., *274:* 26113–26119, 1999.
22. Chini, B., Clementi, F., Hukovic, N., and Sher, E. Neuronal-type α-bungarotoxin receptors and the α 5-nicotinic receptor subunit gene are expressed in neuronal and nonneuronal human cell lines. Proc. Natl. Acad. Sci. USA, *89:* 1572–1576, 1992.
23. Heusch, W. L., and Maneckjee. R Signalling pathways involved in nicotine regulation of apoptosis of human lung cancer cells Carcinogenesis (Lond.), *19:* 551–556, 1998.
24. Frodin, M., and Gammeltoft, S. Role and regulation of 90 kDa ribosomal S6 kinase (RSK) in signal transduction. Mol. Cell. Endocrinol., *151:* 65–77, 1999.
25. Lev, S., Moreno, H., Martinez, R., Canoll, P., Peles, E., Musacchio, J. M., Plowman, G. D., Rudy, B., and Schlessinger, J. Protein tyrosine kinase PYK2 involved in Ca(2+)-induced regulation of ion channel and MAP kinase functions. Nature (Lond.), *376:* 737–745, 1995.
26. Farnsworth, C. L., Freshney, N. W., Rosen, L. B., Ghosh, A., Greenberg, M. E., and Feig, L. A. Calcium activation of Ras mediated by neuronal exchange factor Ras-GRF. Nature (Lond.), *376:* 524–527, 1995.
27. Fitzgerald, E. M. Regulation of voltage-dependent calcium channels in rat sensory neurones involves a Ras-mitogen-activated protein kinase pathway. J. Physiol., *527:* 433–444, 2000.
28. Irida, N., Namikawa, K., Kiyama, H., Ueno, H., Nakamura, S., and Hattori, S. Requirement of Ras for the activation of mitogen-activated protein kinase by calcium influx, cAMP, and neurotrophin in hippocampal neurons. J. Neurosc., *21:* 6459–6466, 2001.
29. Lee, F. S., Hagler, J., Chen, Z. J., Maniatis, T. Activation of the IκB α kinase complex by MEKK1, a kinase of the JNK pathway. Cell, *88:* 213–222, 1977.
30. Bertolotto, C., Maulon, L., Filippa, N., Baier, G., and Auberger, P. Protein kinase C θ and ϵ promote T-cell survival by a rsk-dependent phosphorylation and inactivation of BAD. J. Biol. Chem., *275:* 37246–37250, 2000.
31. Dajas-Bailador, F. A., Soliakov, L., and Wonnacott, S. Nicotine activates the extracellular signal-regulated kinase 1/2 via the α7 nicotinic acetylcholine receptor and protein kinase A, in SH-SY5Y cells and hippocampal neurones. J. Neurochem., *80:* 520–530, 2002.
32. Nakayama, H., Numakawa, T., Ikeuchi, T., and Hatanaka, H. Nicotine-induced phosphorylation of extracellular signal-regulated protein kinase and CREB in PC12h cells. J. Neurochem., *79:* 489–498, 2001.
33. Scheid, M. P., Schubert, K. M., and Duronio, V. Regulation of bad phosphorylation and association with Bcl-x(L) by the MAPK/Erk kinase. J. Biol. Chem., *274:* 31108–31113, 1999.
34. Mossman, B., Bignon, J., Corn, M., Seaton, A., and Gee, J. Asbestos: scientific developments and implications for public policy. Science (Wash. DC), *247:* 294–301, 1990.
35. Cummins, A. B., Palmer, C., Mossman, B. T., and Taatjes, D. J. Persistent localization of activated extracellular signal-regulated kinases (ERK1/2) is epithelial cell-specific in an inhalation model of asbestosis. Am. J. Pathol., *162:* 713–720, 2003.
36. Ramos-Nino, M. E., Timblin, C. R., and Mossman, B. T. Mesothelial cell transformation requires increased AP-1 binding activity and ERK-dependent Fra-1 expression. Cancer Res., *62:* 6065–6069, 2002.
37. Bocchetta, M., Miele, L., Pass, H. I., and Carbone, M. Notch-1 induction, a novel activity of SV40 required for growth of SV40-transformed human mesothelial cells. Oncogene, *22:* 81–89, 2003.